Phase diagrams and superconductivity of ternary Na-Al-H compounds at high pressure

Hao Song,[1] Zihan Zhang,[1] Mingyang Du,[1] Qiwen Jiang,[1] Defang Duan,[1,*] and Tian Cui[1,2,†]
[1]*State Key Laboratory of Superhard Materials, College of Physics, Jilin University, Changchun 130012, China*
[2]*Institute of High Pressure Physics, School of Physical Science and Technology, Ningbo University, Ningbo 315211, China*

(Received 30 March 2021; revised 5 September 2021; accepted 8 September 2021; published 21 September 2021)

Invigorated by the high-temperature superconductivity in ternary hydrogen-dominated compounds under high pressures, we systematically explored high-pressure phase diagrams, electronic properties, lattice dynamics, and superconductivity of ternary Na-Al-H systems using *ab initio* methods. We found three stable compounds of $NaAlH_4$, $NaAlH_6$, and $NaAlH_8$, as well as a metastable compound of $NaAlH_7$ under high pressures. Except for $NaAlH_4$, they all containing H^- and H_2 units. Electronic structure calculations reveal that $NaAlH_7$ and $NaAlH_8$ are metallic, while $NaAlH_4$ and $NaAlH_6$ are semiconductors. In addition, $NaAlH_8$ exhibits a phonon anomaly (dip) in multiple phonon branches along the A-M direction. The phonon anomaly induced by Fermi-surface nesting boosts the electron-phonon coupling strength, and as a result, a superconducting transition temperature T_c of 55 K was produced at 300 GPa.

DOI: 10.1103/PhysRevB.104.104509

I. INTRODUCTION

The discovery of materials relevant to high-temperature superconductivity has aroused great interest in the past decades. Metallization of solid hydrogen has been proposed and potential room-temperature superconductivity under high pressures [1]. But the metallization of hydrogen is very hard to achieve, and experimental observations of the metallic hydrogen phase remain controversial. About five decades earlier, introduction of impurities into hydrogen to provide a chemical precompression effect was considered as a method for reducing the metallization pressure of pure hydrogen [2]. But progress took off at the beginning of this century after Ashcroft [3] proposed that hydrogen-rich compounds are an alternative to pursue high-T_c superconductors. In addition, with technical innovation, supercomputer simulations led theorists to predict the properties of various hydrides more conveniently, and the widespread use of compact diamond anvils let experimentalists squeeze the most promising candidates to test their mettle.

Until now, almost all binary hydrides have been investigated by structure searching simulations [4–8]. Research on superconducting binary hydrides are fruitful and corresponding techniques have matured, such as SiH_3 with T_c of 139 K at 275 GPa [9], CaH_6 with T_c of 235 K at 150 GPa [10], YH_6 with T_c of 264 K at 120 GPa [11], HfH_{10} with T_c of 234 K at 250 GPa [12], and TeH_4 with T_c of 104 K at 170 GPa [13]. Significant achievements in hydride superconductivity have been made in H_3S [14–17] and LaH_{10} [18–22]. H_3S adopts a covalent sixfold cubic structure exhibiting a high T_c of 203 K. In LaH_{10}, hydrogen-rich sodalitelike hydrides with an H_{32} cage also exhibit a high T_c of 250 K.

Despite the vast impressive achievements that have been made with regard to binary hydrides under high pressure, physicists have proved most binary hydrides to be dead ends for room-temperature superconductivity. Recently, there were some theoretical studies on the superconductivity of ternary hydrides at high pressures [23–30]. $MgSiH_6$ [24] and $MgGeH_6$ [23] were predicted to be superconductors with T_c of ∼60 K at high pressure. Phosphorus hydrides were predicted to be stable under pressure via additional doped lithium, especially $LiPH_6$ with T_c of 150–167 K at 200 GPa [27]. Li_2MgH_{16} exhibits an unprecedented high T_c of 473 K at 250 GPa by means of theoretical calculation. Experimental studies on ternary hydrides are being carrying out at the same time. Experimentalists found that $BaReH_9$ is a superconductor with T_c about 7 K at 100 GPa [25]. Li_5MoH_{11} can be synthesized under high pressure and shows unexpectedly low $T_c < 10$ K [31]. More recently, the discovery of room-temperature superconductivity in a ternary C-S-H [32] system with T_c about 287 K at 267 GPa is a long-sought scientific milestone in room-temperature superconductivity.

At atmospheric conditions sodium hydrides adopt NaH stoichiometry, which crystallizes in the rock-salt structure. Metallization in sodium hydrides will likely occur because of pressure-induced band overlap, but sodium hydrides are unlikely to have a high density of states at the Fermi level. It is reported that some phases of NaH_n ($n > 1$) with plenty of H_2 units are metallized at lower pressures as a result of partial filling of the H_2 σ_u^* bands by the Na $3s$ electrons [33]. In the aluminum hydrides, the well-studied $Pm\bar{3}$ n phase of AlH_3 is particularly noteworthy [34,35]. Indeed, AlH_3 is not a good metal, judging from the small density of states (DOS) at the Fermi level. The theoretical predicted T_c of the $Pm\bar{3}$ n-AlH_3 rapidly decreases with compression and becomes almost zero above ∼200 GPa. For ternary sodium aluminum hydride, metal-doped $NaAlH_4$ with properties of high hydrogen-storage capacity and reversible dissociation has attracted special interest and been extensively studied as a hydrogen-storage material [36,37].

*Corresponding author: duandf@jlu.edu.cn
†Corresponding author: cuitian@nbu.edu.cn/cuitian@jlu.edu.cn

In this paper we report the results of a first-principles study on the Na-Al-H system within the pressure range of 100–300 GPa. Calculations of electronic properties reveal that $NaAlH_4$ and $NaAlH_6$ are indirect band-gap semiconductors, while $NaAlH_7$ and $NaAlH_8$ containing both H^- and H_2 units are metal. In addition, the phonon anomaly of $NaAlH_8$ induced by the Fermi nesting significantly affects electron-phonon coupling (EPC) strength under high pressures, and $NaAlH_8$ exhibits a superconducting transition temperature T_c of 55 K at 300 GPa. Moreover, our work is important in order to understand the high-pressure phase diagram and basis properties of Na-Al-H ternary systems.

II. COMPUTATIONAL DETAILS

Variable-composition structure searches for $Na_xAl_yH_z$ ($x = 1 \sim 4$, $y = 1 \sim 4$, $z = 1 \sim 12$) were performed at 100, 200, and 300 GPa by the USEXP [38,39] and AIRSS [40,41] codes. Both USPEX and AIRSS are very successful in predicting high-pressure compounds [41,42]. In total, 164 different compositions were considered for the Na-Al-H system, where nearly 120 structures for each stoichiometry were generated in variable-composition structure searches. Furthermore, we focused on hydrogen-rich compositions, and fixed-composition predictions were employed for these selected stoichiometries. Structural relaxation was carried out within the framework of density functional theory as implemented in VASP [43] and CASTEP [44–46]. The interactions between electrons and ions were modeled by using the projector augmented wave (PAW) method [47] with $2p^6 3s^1$, $3s^2 3p^1$, and $1s^1$ treated as valence electrons for Na, Al, and H. The generalized gradient approximation (GGA) in the scheme of Perdew-Burke-Ernzerhof (PBE) and the Heyd, Scuseria, and Ernzerhof (HSE) hybrid functional were chosen for the exchange-correlation functional. A kinetic cutoff energy of 700 eV and Monkhorst-Pack [48] k meshes with grid spacing of $2\pi \times 0.03$ Å^{-1} were adopted to ensure convergence of enthalpy to be better than 1 meV per atom. The calculation of the electron localization function (ELF), which is used to describe and visualize chemical bonds in molecules and solids, was performed with denser k meshes $2\pi \times 0.02$ Å^{-1}. Phonon calculations were carried out by using the supercell approach as implemented by PHONOPY [49]. Superconducting properties and EPC calculations were performed using density functional perturbation theory (DFPT) [50] and the McMillan equation [51] implemented in the Quantum ESPRESSO package [52]. Norm-conserving pseudopotentials of Troullier-Martins (TM) form pseudopotentials [53] were used with a kinetic energy cutoff of 90 Ry. Self-consistent electron density and EPC were evaluated by employing a $24 \times 24 \times 16$ k mesh and Γ-centered $6 \times 6 \times 4$ q mesh for $P4/mmm$-$NaAlH_8$.

III. RESULTS AND DISCUSSION

A. Ternary phase diagrams and different synthetic routes of ternary hydrides

For a ternary system, the precise exploration of properties, such as the stability and superconductivity, is still a challenge, caused by excessive stoichiometric proportions. For the Na-Al-H system, Na-H and Al-H binary compounds have been systematically investigated, and some compounds exhibit superconducting properties under high pressure [33,54]. Here we constructed the ternary phase diagram of Na-Al-H system at 100, 200, and 300 GPa (see Fig. 1 and Fig. S1-2 in the Supplemental Material [55]). For binary hydrides, $Pm\bar{3}$ n-AlH_3, Cc-NaH_7, $Cmc21$-NaH_9, and $P1$-NaH_{11} are consistent with the literature [33,54], and we found the $Fd\bar{3}$ m-NaAl is the only stable compound in the Na-Al system at 100 GPa. As shown in Fig. 1, except for elemental solids and binary compounds, we predicted several stable and metastable ternary hydrides at high pressures: $NaAl_2H_7$, Na_2AlH_7, $NaAlH_4$, $NaAlH_5$, $NaAlH_6$, $NaAlH_7$, and $NaAlH_8$. To the best of our knowledge, some previous studies of ternary systems focus on thermodynamic stable phases [23,24]. However, this is likely a sufficient but not necessary condition for a material to be synthesizable [6]. Many structures observed in high-pressure experiments are metastable phases [56–58]. Some experimentally synthesized metastable compounds even have high positive formation enthalpies with high energy gains larger than 40 meV/atom [59]. This work showed that controlled heating and cooling cycles or pressure-hysteresis cycles permit one to stabilize different metastable phases selectively. At 300 GPa, $NaAlH_7$ above the convex hull less than

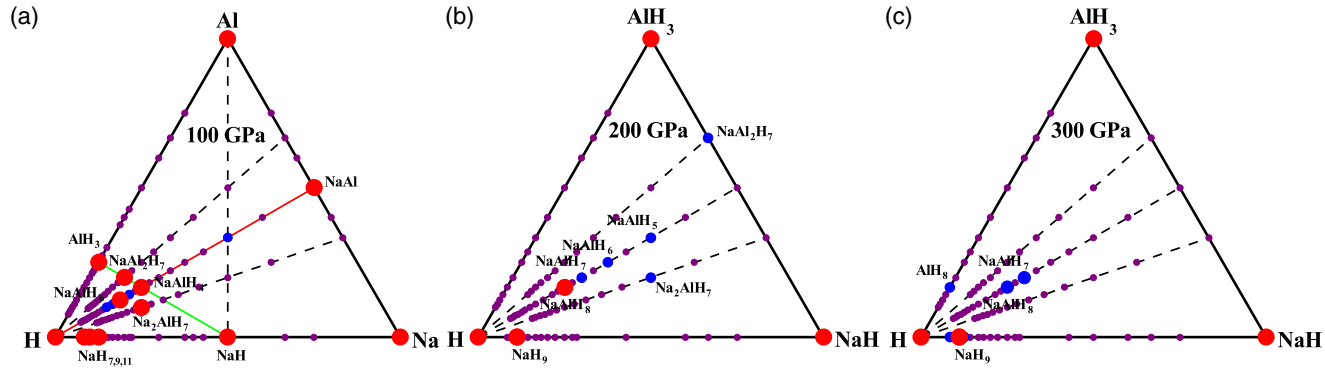

FIG. 1. Convex hull of Na-Al-H system at 100 GPa (a) relative to elemental Na, Al, and H, convex hull at 200 GPa (b) and 300 GPa (c) relative to NaH, AlH_3, and H. Red, blue, and purple circles indicate stable, metastable (with formation enthalpies below 50 meV/atom), and unstable phases, respectively.

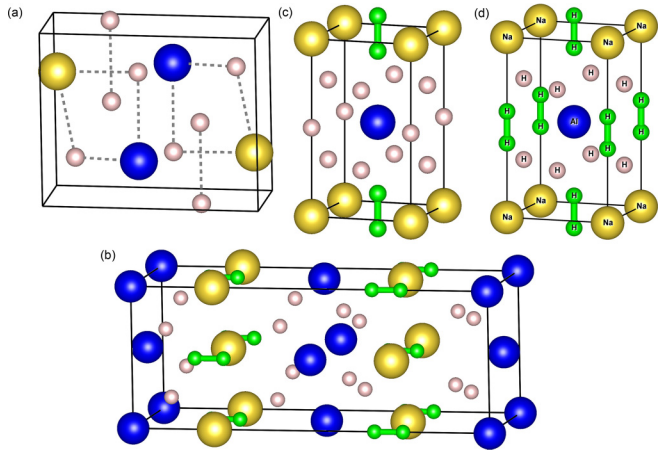

FIG. 2. The crystal structures of (a) $P2_1/m$-$NaAlH_4$, (b) *Aba*2-$NaAlH_6$, (c) *P4/mmm*-$NaAlH_7$, and (d) *P4/mmm*-$NaAlH_8$. Sodium atoms are colored yellow, aluminum atoms are blue, isolated hydridic (H^-) hydrogen atoms are pink, and H_2 units are green.

11 meV/atom is metastable [see Fig. 1(c)], and this does not preclude $NaAlH_7$ from experimental synthesis.

To further get more information about phase transition, we calculated the enthalpies of several structures in $NaAlH_4$, $NaAlH_6$, $NaAlH_7$, and $NaAlH_8$ from 50 to 300 GPa, as shown in Fig. S3. Note that there is no phase transformation for $NaAlH_4$ (space group $P2_1/m$) and $NaAlH_6$ (space group *Aba*2). As for the metastable compound $NaAlH_7$, there are two energetically competing phases (see Fig. S3 in the Supplemental Material [55]), and in terms of our calculation, the enthalpy of the *P4/mmm* phase is slightly lower than the *Cmmm* phase. Although there is a phase transformation at 75 GPa for $NaAlH_8$, we found it is thermodynamically stable only from 160 to 290 GPa (convex hull), so we only concerned the *P4/mmm* phase. The crystal structures of hydrides mentioned above are depicted in Fig. 2, and the detailed information of structure parameters is listed in Table S2 of the Supplemental Material [55].

Due to abundant precursors (Na, Al, H, AlH_3, NaH, and NaAl), ternary Na-Al-H hydrides can be synthesized by different synthetic routes at high pressure, for example, $Na + Al + H_2$, $Na + AlH_3 + H_2$, $NaH + Al + H_2$, $NaH + AlH_3 + H_2$, and $NaAl + 2H_2$. In Fig. 1(a), two different color lines (red and green) intersect at $NaAlH_4$, indicating that it could be synthetized by two different synthetic routes ($NaAl + 2H_2 \rightarrow NaAlH_4$ and $NaH + AlH_3 \rightarrow NaAlH_4$). Here we are mainly concerned with four potential synthetic routes ($Na + Al + H_2$, $Na + AlH_3 + H_2$, $NaH + Al + H_2$, $NaH + AlH_3 + H_2$) and calculated their formation enthalpies as shown in Table I. At 200 GPa, *P4/mmm*-$NaAlH_8$ always possesses negative formation enthalpies, indicating the thermodynamic stability. Comparing the formation enthalpies of multiple synthetic routes, compressing mixtures of $NaH + AlH_3 + H_2$ is the most energetically favorable route to synthesis $NaAlH_n$ (see Table I). Seen from another aspect, $NaAlH_n$ ($n > 4$) also can be synthesized by squeezing $NaAlH_4 + H_2$. We think that some other synthetic routes are possibly attained by extending the precursors or varying combinations, but this requires greater computational costs.

TABLE I. Formation enthalpies (eV/atom) of $NaAlH_n$ at 100, 200, and 300 GPa. ΔH_1, ΔH_2, ΔH_3, and ΔH_4 represent the decomposition of $NaAlH_n$ into Na+Al+H, $Na + AlH_3 + H_2$, $NaH + Al + H_2$, and $NaH + AlH_3 + H_2$, respectively.

		ΔH_1	ΔH_2	ΔH_3	ΔH_4
100 GPa	Na_2AlH_7	−0.756	−0.611	−0.218	−0.073
	$NaAlH_4$	−0.723	−0.481	−0.275	−0.034
	$NaAlH_6$	−0.558	−0.377	−0.222	−0.041
	$NaAl_2H_7$	−0.577	−0.287	−0.308	−0.018
200 GPa	$NaAlH_5$	−0.825	−0.472	−0.319	0.034
	$NaAlH_6$	−0.729	−0.419	−0.286	0.024
	$NaAlH_7$	−0.670	−0.395	−0.276	−0.001
	$NaAlH_8$	−0.619	−0.371	−0.264	−0.017
300 GPa	$NaAlH_7$	−0.827	−0.473	−0.341	−0.006
	$NaAlH_8$	−0.761	−0.441	−0.361	−0.022

Provided that these specific synthetic routes are determined, they will be very helpful to further stimulate experimental synthesis.

B. Electronic properties of $NaAlH_n$

The electronic band structure and density of electronic states of $NaAlH_4$, $NaAlH_6$, $NaAlH_7$, and $NaAlH_8$ at high pressure are calculated and shown in Fig. 3. The $P2_1/m$-$NaAlH_4$ is an indirect wide-band-gap semiconductor at 100 GPa, and the band-gap E_g is about 3.6 eV, which narrowed to 2.9 eV at 200 GPa (see Table S1 in the Supplemental Material [55]). *Aba*2-$NaAlH_6$ is also an indirect band-gap semiconductor at 100 GPa [see Fig. 3(b)] with $E_g = 3.1$ eV. For the semiconductors $NaAlH_4$ and $NaAlH_6$, we calculated the electronic band structures using HSE functionals, as depicted in Fig. S4. For $NaAlH_4$ at 100 GPa, the valence-band maximum (VBM) is lowered by 0.71 eV and the conduction-band minimum (CBM) is raised by 0.37 eV compared to PBE functionals. For $NaAlH_6$ at 200 GPa, the VBM is lowered by 0.6 eV and the CBM is raised by 0.3 eV compared to PBE functionals. The lowering of the VBM in HSE functionals can be attributed to the reduced self-interaction for the H 1*s*-derived states that compose the upper part of the valence band. The upward shift of the CBM is also expected, since Hartree-Fock generally increases band gaps. $NaAlH_7$ and $NaAlH_8$ both are metallic with significant hydrogen contribution to the electronic DOS at the Fermi level. The H-derived electronic density of states at the Fermi level indicated electron-phonon coupling was generated mainly by hydrogen electrons coupling with phonon modes. There are three bands crossing the Fermi level for $NaAlH_7$, four bands for $NaAlH_8$. Excluding this difference, we can see the band structures of $NaAlH_7$ and $NaAlH_8$ are quite similar. The extra band crossing the Fermi level of $NaAlH_8$ is directly caused by the Fermi level increase and the increase of Fermi energy caused by the extra electron from extra hydrogen. More intriguingly, even though there is one more hydrogen in the $NaAlH_8$ compound, the DOS of $NaAlH_7$ is about twice larger than $NaAlH_8$. We think that the extra hydrogen has a reverse effect—it bonded

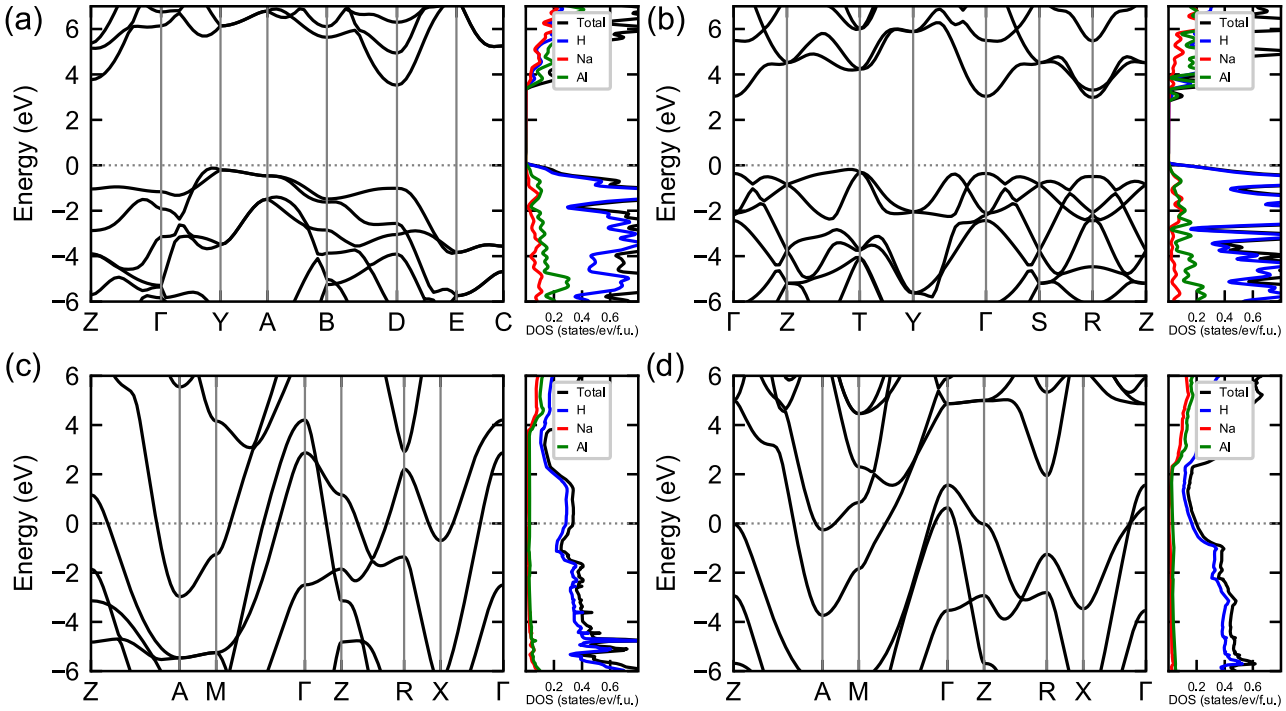

FIG. 3. The band structures and partial electronic density of states (PDOS) of (a) $P2_1/m$-$NaAlH_4$ at 100 GPa and (b) *AbA*2-$NaAlH_6$ at 100 GPa using the HSE functionals, (c) *P4/mmm*-$NaAlH_7$ at 200 GPa, and (d) *P4/mmm*-$NaAlH_8$ at 200 GPa using the GGA-PBE functionals.

to an isolated hydrogen and caused the reduction of free electrons.

The chemical bonding of $NaAlH_n$ ($n \geqslant 4$) was examined by the ELFs and Bader charge analysis. The ELF of $NaAlH_{6,7,8}$ were calculated and depicted in Fig. 4 and Fig. S7 in the Supplemental Material [55]. There is no charge localization between Na-H, Al-H, indicating the bondings are ionic. The ELF value for H_2 units is bigger than 0.75, showing the evidence for covalent bonding. In Table II, Bader charge analysis reveals that charges transfer from Na and Al to isolated H and H_2 units. Na and Al lose no less than 0.70 *e* and 2.30 *e* charges, respectively, in the $NaAlH_n$ ($n = 4$, 6, 7, 8) compound. Each isolated H gains about 0.6 $\sim$ 0.8 *e* forming the H^- entity. H_2 unit gains about 0.14 *e*, 0.29 *e*, and 0.27 *e* charges in $NaAlH_6$, $NaAlH_7$, and $NaAlH_8$, respectively. The H_2 unit in $NaAlH_7$ and $NaAlH_8$ gains about twice more charges as in $NaAlH_6$. In addition, interatomic distances of H_2 units in $NaAlH_n$ ($n = 6,7,8$) are shown in Table S3; $NaAlH_7$ has the maximum distances (0.81 Å) of H_2 units in $NaAlH_n$, and we also know that the H_2 unit in $NaAlH_7$ gains the maximum charges from Na and Al. We think that the additional electrons reside in the H-H antibonding orbital and therefore weaken the H-H bonding, thus increasing the H-H distance, which results in longer H-H distance compared to that in free H_2 molecules (see Table S3 in the Supplemental Material [55]). However, the relationship between H-H distances and additional electrons is not monotonic in $NaAlH_n$. The H-H distances of H_2 units in $NaAlH_6$ and $NaAlH_8$ are comparable at 200 GPa, which is about 0.78 Å, while H_2 units in $NaAlH_8$ gain almost twice more charges than those in $NaAlH_6$. According to the metallization of Na-H systems [33] and AlH_3 [34], there are two strategies for the metallization of $NaAlH_{7,8}$: (i) electrons transfer from Na and Al to H_2 units, partially filling the H_2 σ_u^* bands caused metallization, and (ii) a pressure-induced overlap of H^- and H_2 σ_u^* bands.

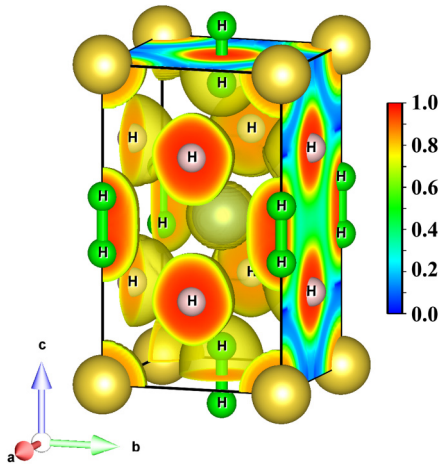

FIG. 4. Electronic localization function (ELF) of *P4/mmm*-$NaAlH_8$ at 200 GPa.

C. Phonon dispersion and superconductivity properties of $NaAlH_n$

Phonon calculations were performed for $NaAlH_4$, $NaAlH_6$, $NaAlH_7$, and $NaAlH_8$. The absence of imaginary frequencies in the whole Brillouin zone for the compounds is clearly

TABLE II. Bader analysis for $NaAlH_{4,6,7,8}$ at 100 and 200 GPa.

	100 GPa		200 GPa		
$\delta(e)$	$NaAlH_4$	$NaAlH_6$	$NaAlH_6$	$NaAlH_7$	$NaAlH_8$
H	−0.72∼ −0.80	−0.72∼ −0.76	−0.71∼ −0.75	−0.61∼ −0.62	−0.64
H_2		−0.14	−0.14	−0.29	−0.27
Na	0.75	0.75	0.71	0.72	0.73
Al	2.31	2.33	2.33	2.36	2.37

evidence for dynamical stability (see Fig. 5 and Figs. S8 and S9 in the Supplemental Material [55]). As expected, owing to the discrepancy of atomic mass and existing forms of H atoms, the vibrational modes were divided into different parts. For $NaAlH_4$, the vibrational modes were divided into two parts (see Fig. S8 in the Supplemental Material [55]), the low-frequency branches were associated with the vibrations of both Na and Al, whereas the higher frequency branches were mainly associated with H atoms. While the vibrational modes of $NaAlH_{6,7,8}$ can be divided into three parts (see Fig. 5 and Fig. S9 in the Supplemental Material [55]), the low-frequency modes also dominated by Na and Al atoms, the middle parts related to both H_2 units and H atoms, and the high ends of the vibrational modes related to the motions of H_2 units.

Figure 5 presents the phonon dispersion, projected phonon density of states (PHDOS), the Eliashberg spectral function $\alpha^2F(\omega)$, and the EPC integrated $\lambda(\omega)$ of $NaAlH_8$ at 200 and 300 GPa. The most noteworthy feature in the phonon dispersion is the presence of slight anomalies (dip) mainly concentrated in the middle parts of vibration modes (especially the ninth vibration mode) along A-M. Many optical branches associated with vibrations of H_2 units exhibit dips (anomalous phonon) at specific high-symmetry points A and M. And these branches deepen strongly with decreasing pressure, as shown in Fig. 5. To clearly elucidate the reason of this anomalous dip, we investigated the Fermi-surface nesting in the $NaAlH_8$ by applying the nesting function:

$$(Q) = \frac{1}{N}\sum_{\vec{k},i,j}\delta(\varepsilon_{\vec{k},i} - \varepsilon_F)\delta(\varepsilon_{\vec{k}+\vec{Q},j} - \varepsilon_F), \qquad (1)$$

where $\varepsilon_{k,i}$ indicate the Kohn-Sham eigenvalues and i, j are the indices of energy bands, respectively, ε_F denotes the

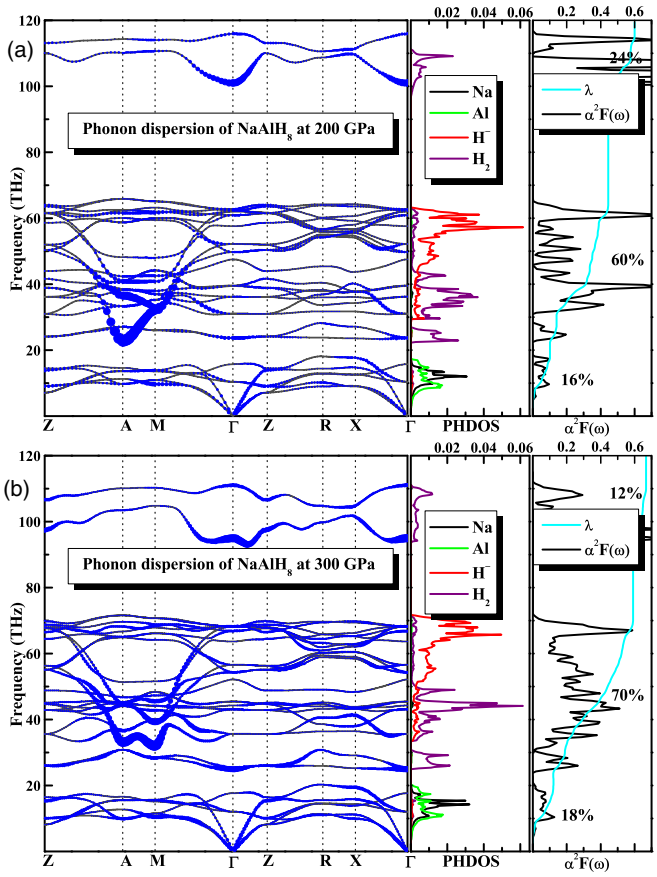

FIG. 5. Phonon dispersion, corresponding density of states, Eliashberg spectral function $\alpha^2F(\omega)$, and EPC integrated $\lambda(\omega)$ of $NaAlH_8$ at 200 and 300 GPa. These blue solid circles projected on phonon dispersion curves show electron-phonon coupling (EPC), and sizes of circles are proportional to EPC strength.

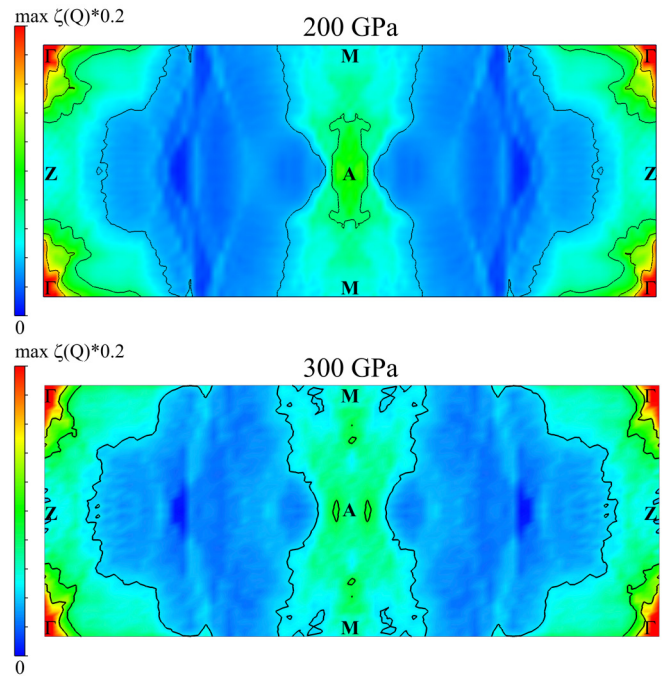

FIG. 6. The nesting function of *P4/mmm*-$NaAlH_8$ at 200 (top panel) and 300 GPa (lower panel).

TABLE III. The calculated EPC parameter λ, logarithmic average phonon frequency $\omega_{\log}$ (K), electronic density of states at Fermi level $N(\varepsilon_f)$ (states/spin/Ry/f.u.), and superconducting transition temperatures T_c (K) with $\mu^* = 0.1$–0.13 at corresponding pressures P (GPa).

Structure	P (GPa)	λ	$\omega_{\log}$	$N(\varepsilon_f)$	T_c (K)
P4/mmm $NaAlH_8$	200	0.61	1600	2.2	28–39
	250	0.66	1724	2.2	39–45
	300	0.66	1842	2.2	41–55

Fermi energy, and N is the number of k points (k mesh is $100 \times 100 \times 100$). Figure 6 shows a cross section of $\zeta(Q)$ along the high-symmetry lines Γ-Z-A-M. The appearance of green areas in Fig. 6 indicates the occurrence of Fermi-surface nesting. For the Γ point, its $\zeta(Q)$ represents the entire Fermi surface nests into itself, which has no actual physical meaning. In order to clearly show the Fermi-surface nesting areas, we cut the redundant peak at Γ point. The $\zeta(Q)$ quantitatively describes peaks along A-M directions (green areas), demonstrating that strong Fermi-surface nesting occurs at these directions. Along the A-M directions, peaks of the $\zeta(Q)$ can be attributed to Kohn anomalies [60]. To the best of our knowledge, Kohn anomaly is a special case of Fermi-surface nesting which may occur only for q such that are two electronic states k_1 and $k_2 = k_1 + q$, both on the Fermi surface. The regions of phonon softening correspond to the nesting directions, strongly indicating phonon softening is induced by Fermi-surface nesting or Kohn anomalies. And it is clearly seen that the EPC strength is particularly enhanced in these regions of phonon dips. As is well known, stronger EPC strength is favorable to produce a high superconducting critical temperature T_c. In addition, from PHDOS of $NaAlH_8$, it is found that the positions of peaks in PHDOS derived from Na and Al atoms are similar, which is ascribed to similar atomic masses and positions.

The spectral function $\alpha^2F(\omega)$ and the EPC integrated $\lambda(\omega)$ are also shown in Fig. 5. At 200 GPa, it was found that the low-frequency, middle-frequency, and high-frequency EPC contribute 16%, 60%, and 24% to total EPC λ, respectively. At 300 GPa, the proportion is 18%, 70%, and 12%, respectively. Herein it is noted that the middle part of vibrational modes provides very important contributions to EPC. In other words, the H and H_2-derived frequency contribute 84% and 82% of the total λ at 200 and 300 GPa, respectively, which is common in binary hydrides containing H_2 units. T_c was calculated based on the spectral function $\alpha^2F(\omega)$ by solving the Allen-Dynes modified McMillan equation [51]:

$$T_c = \frac{\omega_{log}}{1.2} \exp\left[-\frac{1.04(1+\lambda)}{\lambda - \mu^*(1+0.62\lambda)}\right], \quad (2)$$

with Coulomb pseudopotential $\mu^* = 0.1$–0.13. For $\lambda < 1.5$, this equation can provide a highly accurate value of T_c. As listed in Table III, the electron-phonon coupling coefficient λ is 0.66, the logarithmic average phonon frequency $\omega_{\log}$ is 1842 K, and T_c is 55 K at 300 GPa. As pressure increase, phonon tends to harden and $\omega_{\log}$ raises, and the EPC parameter λ is basically unchanged, as a result, the T_cs slightly increase.

IV. CONCLUSION

In summary, we investigated the high-pressure phase diagram, electronic properties, lattice dynamics, and superconductivity of ternary Na-Al-H systems. We have identified several stable and metastable compounds under high pressure: $NaAlH_4$, $NaAlH_6$, $NaAlH_7$, $NaAlH_8$, etc. At 300 GPa, the superconducting transition temperature of $NaAlH_8$ is 55 K. The phonon anomaly (dip) in many phonon branches along the A-M direction, which is induced by Fermi-surface nesting boosting the EPC strength, playing an important role in superconductivity. In addition, we propose four potential synthetic routes for Na-Al-H compounds which will provide a reference for further experimental study. This work may shed light on the design principles for other high-temperature superconducting hydrides.

ACKNOWLEDGMENTS

This work was supported by the National Key R&D Program of China (Grant No. 2018YFA0305900) and the National Natural Science Foundation of China (Grants No. 12122405, No. 52072188, and No. 51632002). Parts of the calculations were performed in the High Performance Computing Center (HPCC) of Jilin University and TianHe-1(A) at the National Supercomputer Center in Tianjin.

[1] N. W. Ashcroft, Phys. Rev. Lett. **21**, 1748 (1968).
[2] J. J. Gilman, Phys. Rev. Lett. **26**, 546 (1971).
[3] N. W. Ashcroft, Phys. Rev. Lett. **92**, 187002 (2004).
[4] T. Bi, N. Zarifi, T. Terpstra, and E. Zurek, *Reference Module in Chemistry, Molecular Sciences and Chemical Engineering* (Elsevier, 2019).
[5] D. F. Duan, Y. X. Liu, Y. B. Ma, Z. Shao, B. B. Liu, and T. Cui, Natl. Sci. Rev. **4**, 121 (2017).
[6] J. A. Flores-Livas, L. Boeri, A. Sanna, G. Profeta, R. Arita, and M. Eremets, Phys. Rep. **856**, 1 (2020).
[7] D. V. Semenok, I. A. Kruglov, I. A. Savkin, A. G. Kvashnin, and A. R. Oganov, Curr. Opin. Solid State Mater. Sci. **24**, Unsp 100808 (2020).
[8] D. F. Duan, H. Y. Yu, H. Xie, and T. Cui, J. Supercond. Novel Magn. **32**, 53 (2019).
[9] X. Jin, X. Meng, Z. He, Y. Ma, B. Liu, T. Cui, G. Zou, and H. K. Mao, Proc. Natl. Acad. Sci. USA **107**, 9969 (2010).
[10] H. Wang, S. T. John, K. Tanaka, T. Iitaka, and Y. Ma, Proc. Natl. Acad. Sci. USA **109**, 6463 (2012).
[11] Y. W. Li, J. Hao, H. Y. Liu, J. S. Tse, Y. C. Wang, and Y. M. Ma, Sci. Rep. **5**, 9948 (2015).

[12] H. Xie, Y. Yao, X. Feng, D. Duan, H. Song, Z. Zhang, S. Jiang, S. A. T. Redfern, V. Z. Kresin, C. J. Pickard, and T. Cui, Phys. Rev. Lett. **125**, 217001 (2020).

[13] X. Zhong, H. Wang, J. Zhang, H. Liu, S. Zhang, H.-F. Song, G. Yang, L. Zhang, and Y. Ma, Phys. Rev. Lett. **116**, 057002 (2016).

[14] D. F. Duan, Y. Liu, F. Tian, D. Li, X. Huang, Z. Zhao, H. Yu, B. Liu, W. Tian, and T. Cui, Sci. Rep. **4**, 6968 (2014).

[15] D. F. Duan, X. Huang, F. Tian, D. Li, H. Yu, Y. Liu, Y. Ma, B. Liu, and T. Cui, Phys. Rev. B **91**, 180502(R) (2015).

[16] A. P. Drozdov, M. I. Eremets, I. A. Troyan, V. Ksenofontov, and S. I. Shylin, Nature (London) **525**, 73 (2015).

[17] M. Einaga, M. Sakata, T. Ishikawa, K. Shimizu, M. I. Eremets, A. P. Drozdov, I. A. Troyan, N. Hirao, and Y. Ohishi, Nat. Phys. **12**, 835 (2016).

[18] H. Liu, I. I. Naumov, R. Hoffmann, N. W. Ashcroft, and R. J. Hemley, Proc. Natl. Acad. Sci. USA **114**, 6990 (2017).

[19] F. Peng, Y. Sun, C. J. Pickard, R. J. Needs, Q. Wu, and Y. Ma, Phys. Rev. Lett. **119**, 107001 (2017).

[20] I. Errea, F. Belli, L. Monacelli, A. Sanna, T. Koretsune, T. Tadano, R. Bianco, M. Calandra, R. Arita, F. Mauri, and J. A. Flores-Livas, Nature (London) **578**, 66 (2020).

[21] A. P. Drozdov, P. P. Kong, V. S. Minkov, S. P. Besedin, M. A. Kuzovnikov, S. Mozaffari, L. Balicas, F. F. Balakirev, D. E. Graf, V. B. Prakapenka, E. Greenberg, D. A. Knyazev, M. Tkacz, and M. I. Eremets, Nature (London) **569**, 528 (2019).

[22] M. Somayazulu, M. Ahart, A. K. Mishra, Z. M. Geballe, M. Baldini, Y. Meng, V. V. Struzhkin, and R. J. Hemley, Phys. Rev. Lett. **122**, 027001 (2019).

[23] Y. B. Ma, D. F. Duan, Z. J. Shao, D. Li, L. Y. Wang, H. Y. Yu, F. B. Tian, H. Xie, B. B. Liu, and T. Cui, Phys. Chem. Chem. Phys. **19**, 27406 (2017).

[24] Y. B. Ma, D. F. Duan, Z. J. Shao, H. Y. Yu, H. Y. Liu, F. B. Tian, X. L. Huang, D. Li, B. B. Liu, and T. Cui, Phys. Rev. B **96**, 144518 (2017).

[25] T. Muramatsu, W. K. Wanene, M. Somayazulu, E. Vinitsky, D. Chandra, T. A. Strobel, V. V. Struzhkin, and R. J. Hemley, J. Phys. Chem. C **119**, 18007 (2015).

[26] E. A. Vinitsky, T. Muramatsu, M. Somayazulu, W. K. Wanene, Z. X. Liu, D. Chandra, and R. J. Hemley, J. Phys.: Condens. Matter **28**, 505701 (2016).

[27] Z. Shao, D. Duan, Y. Ma, H. Yu, H. Song, H. Xie, D. Li, F. Tian, B. Liu, and T. Cui, npj Comput. Mater. **5**, 104 (2019).

[28] H. Xie, D. Duan, Z. Shao, H. Song, Y. Wang, X. Xiao, D. Li, F. Tian, B. Liu, and T. Cui, J. Phys.: Condens. Matter **31**, 245404 (2019).

[29] Y. Sun, J. Lv, Y. Xie, H. Liu, and Y. Ma, Phys. Rev. Lett. **123**, 097001 (2019).

[30] C. Kokail, W. von der Linden, and L. Boeri, Phys. Rev. Mater. **1**, 074803 (2017).

[31] D. Meng, M. Sakata, K. Shimizu, Y. Iijima, H. Saitoh, T. Sato, S. Takagi, and S.-i. Orimo, Phys. Rev. B **99**, 024508 (2019).

[32] E. Snider, N. Dasenbrock-Gammon, R. McBride, M. Debessai, H. Vindana, K. Vencatasamy, K. V. Lawler, A. Salamat, and R. P. Dias, Nature (London) **586**, 373 (2020).

[33] P. Baettig and E. Zurek, Phys. Rev. Lett. **106**, 237002 (2011).

[34] C. J. Pickard and R. J. Needs, Phys. Rev. B **76**, 144114 (2007).

[35] I. Goncharenko, M. I. Eremets, M. Hanfland, J. S. Tse, M. Amboage, Y. Yao, and I. A. Trojan, Phys. Rev. Lett. **100**, 045504 (2008).

[36] B. Bogdanovic, R. A. Brand, A. Marjanovic, M. Schwickardi, and J. Tolle, J. Alloys Compd. **302**, 36 (2000).

[37] X. F. Zhou, X. Dong, Z. Zhao, A. R. Oganov, Y. Tian, and H. T. Wang, Appl. Phys. Lett. **100**, 061905 (2012).

[38] A. R. Oganov and C. W. Glass, J. Chem. Phys. **124**, 244704 (2006).

[39] A. O. Lyakhov, A. R. Oganov, H. T. Stokes, and Q. Zhu, Comput. Phys. Commun. **184**, 1172 (2013).

[40] C. J. Pickard and R. J. Needs, J. Phys.: Condens. Matter **23**, 053201 (2011).

[41] C. J. Pickard and R. J. Needs, Phys. Rev. Lett. **97**, 045504 (2006).

[42] A. G. Kvashnin, D. V. Semenok, I. A. Kruglov, I. A. Wrona, and A. R. Oganov, ACS Appl. Mater. Interfaces **10**, 43809 (2018).

[43] G. Kresse and J. Furthmüller, Comput. Mater. **6**, 15 (1996).

[44] M. D. Segall, P. J. D. Lindan, M. J. Probert, C. J. Pickard, P. J. Hasnip, S. J. Clark, and M. C. Payne, J. Phys.: Condens. Matter **14**, 2717 (2002).

[45] M. C. Payne, M. P. Teter, D. C. Allan, T. A. Arias, and J. D. Joannopoulos, Rev. Mod. Phys. **64**, 1045 (1992).

[46] S. J. Clark, M. D. Segall, C. J. Pickard, P. J. Hasnip, M. J. Probert, K. Refson, and M. C. Payne, Z. Kristallogr. **220**, 567 (2005).

[47] G. Kresse and D. Joubert, Phys. Rev. B **59**, 1758 (1999).

[48] H. J. Monkhorst and J. D. Pack, Phys. Rev. B **13**, 5188 (1976).

[49] A. Togo and I. Tanaka, Scr. Mater. **108**, 1 (2015).

[50] S. Baroni, S. de Gironcoli, A. Dal Corso, and P. Giannozzi, Rev. Mod. Phys. **73**, 515 (2001).

[51] P. B. Allen and R. C. Dynes, Phys. Rev. B **12**, 905 (1975).

[52] P. Giannozzi, S. Baroni, N. Bonini, M. Calandra, R. Car, C. Cavazzoni, D. Ceresoli, G. L. Chiarotti, M. Cococcioni, I. Dabo *et al.*, J. Phys.: Condens. Matter **21**, 395502 (2009).

[53] N. Troullier and J. L. Martins, Phys. Rev. B **43**, 1993 (1991).

[54] K. Abe, Phys. Rev. B **100**, 174105 (2019).

[55] See Supplemental Material at http://link.aps.org/supplemental/10.1103/PhysRevB.104.104509 for explicit structural information of the Na-Al-H compounds, as well as additional results about the convex hull diagram, phonon dispersion, and electronic properties.

[56] J. S. C. Kearney, M. Graužinytė, D. Smith, D. Sneed, C. Childs, J. Hinton, C. Park, J. S. Smith, E. Kim, S. D. S. Fitch, A. L. Hector, C. J. Pickard, J. A. Flores-Livas, and A. Salamat, Angew. Chem., Int. Ed. **57**, 11623 (2018).

[57] J. A. Flores-Livas, A. Sanna, A. P. Drozdov, L. Boeri, G. Profeta, M. Eremets, and S. Goedecker, Phys. Rev. Mater. **1**, 024802 (2017).

[58] D. Campanini, Z. Diao, and A. Rydh, Phys. Rev. B **97**, 184517 (2018).

[59] Y. Hinuma, T. Hatakeyama, Y. Kumagai, L. A. Burton, H. Sato, Y. Muraba, S. Iimura, H. Hiramatsu, I. Tanaka, H. Hosono, and F. Oba, Nat. Commun. **7**, 11962 (2016).

[60] W. Kohn, Phys. Rev. Lett. **2**, 393 (1959).